

The East Greenland Spill Jet*

ROBERT S. PICKART, DANIEL J. TORRES, AND PAULA S. FRATANTONI

Woods Hole Oceanographic Institution, Woods Hole, Massachusetts

(Manuscript received 6 July 2004, in final form 3 November 2004)

ABSTRACT

High-resolution hydrographic and velocity measurements across the East Greenland shelf break south of Denmark Strait have revealed an intense, narrow current banked against the upper continental slope. This is believed to be the result of dense water cascading over the shelf edge and entraining ambient water. The current has been named the East Greenland Spill Jet. It resides beneath the East Greenland/Irminger Current and transports roughly 2 Sverdrups of water equatorward. Strong vertical mixing occurs during the spilling, although the entrainment farther downstream is minimal. A vorticity analysis reveals that the increase in cyclonic relative vorticity within the jet is partly balanced by tilting vorticity, resulting in a sharp front in potential vorticity reminiscent of the Gulf Stream. The other components of the Irminger Sea boundary current system are described, including a presentation of absolute transports.

1. Introduction

The first detailed study of the circulation and water masses south of Denmark Strait was carried out in the mid-nineteenth century by the Danish Admiral Carl Ludvig Christian Irminger, after whom the sea is named (Fiedler 2003). Among other things, Irminger determined that Atlantic-origin water flowed northward into the strait west of Iceland, while cold Arctic-origin water flowed equatorward along the continental boundary of Greenland. Not long after this, Hamberg (1884) noted that warm and salty Atlantic water also resided below and offshore of the polar water. Using measurements from the 1895–96 *Ingolf* expeditions, Knudsen (1899) then deduced that the northward-flowing Irminger Current bifurcated south of Denmark Strait, with much of the Atlantic water recirculating to join the “East Greenland Polar Current.”¹ Hence, more than a century ago there existed a rudimentary upper-layer circulation scheme for the Irminger Sea boundary

current system—one that is remarkably accurate even by today’s standards (see Fig. 1).

Since these early measurements there have been numerous field programs that have focused on the hydrography and circulation of the East Greenland shelf and slope. This was driven originally, in part, by the unique topography of the shelf, which contains a series of deep basins and associated banks, making it an important location for trawling of deep-sea fish (e.g., Dietrich 1964). One particularly impressive program was the German expedition on the R/V *Meteor* in 1933 and 1935, which consisted of a set of “spoke wheel” sections around the southern tip of Greenland. From these data Defant (1936) mapped out the path of the East Greenland/Irminger hydrographic front as it progressed around Cape Farewell, more or less trapped to the shelf break. Earlier, Defant (1930) had noted that intrusions of warm and salty Irminger water were regularly found onshore of the front, likely because of eddy formation. Such meandering of the East Greenland/Irminger Current was also discussed by Dietrich (1957a,b) and Blindheim (1968); Lee (1968a) noted significant amounts of Irminger water on the shelf as well. Dietrich (1957a) hypothesized that pumping of nutrients would occur because of the frontal secondary circulation, with ramifications for the distribution of plankton and fish populations. Dietrich (1957a) rightly realized the need for more closely spaced stations to investigate this phenomenon properly.

Other major initiatives investigating the East Greenland/Irminger Current were the IGY program in 1957–58 (Dietrich 1964), the NORWESTLANT program in 1963 (Lee 1968a), the extensive Norwegian study from

¹ This current has also been referred to historically as the East Greenland stream, cold stream, polar stream, Arctic current, and polar current. Today it is referred to as the East Greenland Current.

* Woods Hole Oceanographic Institution Contribution Number 11260.

Corresponding author address: Dr. Robert S. Pickart, Woods Hole Oceanographic Institution, Department of Physical Oceanography, Mail Stop #21, Woods Hole, MA 02543.
E-mail: rpickart@whoi.edu

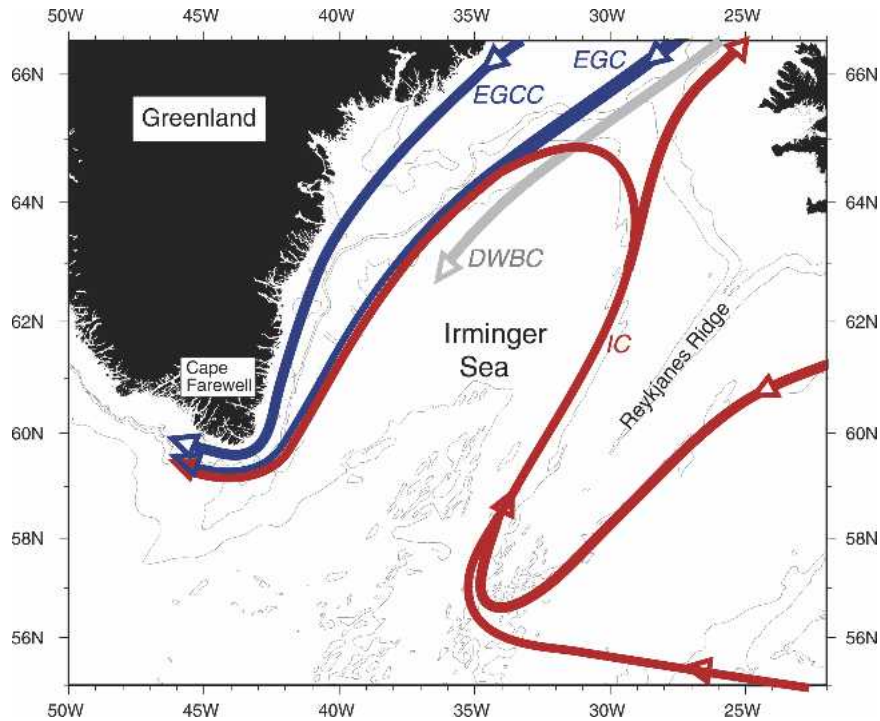


FIG. 1. Schematic of the boundary currents of the Irminger Sea. Red (blue) indicates a warm (cold) upper-layer current. The northward-flowing Irminger Current (IC) on the western flank of the Reykjanes Ridge is fed by two branches of warm water: one recirculating from the eastern flank of the ridge and another from farther south (see Bower et al. 2002; Jakobsen et al. 2003; Pollard et al. 2004). Near Denmark Strait the Irminger Current bifurcates; its northward extension is called the Icelandic Irminger Current (Jonsson and Briem 2003), and the recirculating component merges with the cold East Greenland Current (EGC). We refer to this combined flow—which is associated with a sharp hydrographic front—as the East Greenland/Irminger Current or shelfbreak jet. A separate southward-flowing band of cold water resides on the inner shelf, which Bacon et al. (2002) called the East Greenland Coastal Current (EGCC); we adopt this terminology as well. The deep western boundary current (DWBC) carrying Denmark Strait overflow water is indicated by the gray line (the contribution from the Gibbs Fracture zone is not shown). The bathymetric contours are 500, 1000, 2000, and 3000 m.

1959–64 (Blindheim 1968), and the Irminger Sea Project in 1963–65 (Malmberg et al. 1967). The seasonal coverage and spatial extent of these surveys varied, but like the early *Meteor* cruises noted above, the pattern of hydrographic stations generally provided good along-stream coverage of the current system. The Norwegian study is noteworthy because it contained repeated surveys over several years. Among other things this revealed that the volume of Atlantic water that flows into the sea via the Irminger Current on the western flank of the Reykjanes Ridge fluctuates on interannual time scales, presumably because of winds. Blindheim (1968) suggested that this, rather than changes in the bifurcation of the current at Denmark Strait, would impact the amount of Irminger water flowing southward with the East Greenland/Irminger Current. The NORWESTLANT program concentrated on the seasonal transition from spring to summer and sampled the current system from late March to early August (Lee 1968b). One of the findings showed that there was a

general decrease in salinity of the upper-layer flow as the season progressed, presumably because of ice melt and increased precipitation (Lee 1968a).

In addition to the combined flow of the East Greenland/Irminger Current in the vicinity of the shelf break (Fig. 1), there is an additional branch of the upper-layer Irminger Sea boundary current system located on the inner part of the shelf. This has recently been named the East Greenland Coastal Current by Bacon et al. (2002), although its existence has been known for many years. For example, Malmberg et al. (1967) measured this branch with near-shore current meters (they referred to it as simply the East Greenland Current). Bacon et al. (2002) argue that this branch is driven predominantly by local runoff and ice melt. Recently, the two branches have been distinguished by trajectories of drifters drogued at both 100 m (Krauss 1995) and 15 m (Fratantoni 2001; Reverdin et al. 2003; Jakobsen et al. 2003). It must be remembered, however, that ice cover on the Greenland shelf prohibits the launching of drift-

ers north of Denmark Strait. In Jakobsen's et al. study most of the drifters in the East Greenland Coastal Current originated from the Icelandic slope and shelf (M. Ribergaard 2002, personal communication), likely transported there by wind or eddies in the vicinity of Denmark Strait. Because of the general inaccessibility of the Greenland shelf to in situ measurements, the precise origin and seasonality of the East Greenland Coastal Current are still unknown.

Based on the number of programs over the years, one might think that the kinematics and dynamics of the East Greenland/Irminger Current are well understood at this point. This is not the case, however. In virtually all of the field programs to date the cross-stream resolution of stations has been deficient to resolve properly the detailed structure of the hydrographic front and its associated jet, which, like many other frontal systems around the World Ocean, is complex and time varying. This is partly due to the harsh environment of this region. In addition to the ice cover, which is present on the shelf most of the year, the weather is notoriously nasty (even in summer). Consequently, the majority of historical hydrographic surveys have contained only a few stations in the vicinity of the shelf break, and moored measurements to date have been limited.

In summer 2001 a hydrographic survey was conducted that measured the upper-layer boundary flow of the western Irminger Sea at high resolution (station spacing ≤ 5 km). This detailed view revealed a heretofore undetected component of the boundary current system located at, and just seaward of, the shelf break—beneath the well-known East Greenland/Irminger Current. The feature results from the spilling of dense water over the shelf edge south of Denmark Strait, which forms a narrow gravity current flowing equatorward on the upper continental slope (so narrow that it was missed in previous surveys).² In some ways this is akin to the sinking of dense water through Denmark Strait itself. However, the cascading shelf water is not as dense as the Denmark Strait overflow water (see also Rudels et al. 1999), and the mechanisms leading to the spilling have not yet been determined. We have named this current the East Greenland Spill Jet. The same feature was measured as well in our subsequent survey in 2003.

The purpose of this paper is to introduce and describe the East Greenland Spill Jet using our measurements in 2001, and put this current in context with the East Greenland/Irminger current as well as the deeper flow of Denmark Strait overflow water downstream of the sill. In addition to water property measurements, our field program included vessel-mounted acoustic

Doppler current profiler (ADCP) data obtained at high horizontal resolution. Together with the hydrography, this allows us to compute fields of absolute geostrophic velocity and potential vorticity. After discussing the properties, kinematics, and transport of the different boundary current components in the western Irminger Sea, we focus on the vorticity structure of the spill jet, as well as the entrainment that occurs during its initial adjustment.

2. Field program

a. Hydrographic variables

The hydrographic survey considered here was carried out in August 2001, and included four high-resolution crossings of the East Greenland shelf break (Fig. 2). The intention was to cross the entire shelf on each line, but ice constraints made this impossible since our research vessel was not strengthened for ice breaking. The exception to this was section 3, which coincided with the A1E line of the World Ocean Circulation Experiment (WOCE). On this line we were able to cross most of the shelf, including the East Greenland Coastal Current. However, the focus of this paper is on the two northern lines (sections 1 and 2, Fig. 2) where the East Greenland Spill Jet is first formed.

A Seabird 9+ conductivity/temperature/depth (CTD) system, with dissolved oxygen, was used on a 24×4 L rosette. Water samples were taken for salinity and oxygen. Based on laboratory calibration of the temperature sensors and in situ calibration of the conductivity sensors, the accuracies were 0.001°C and 0.002 (practical salinity scale). In the vicinity of the shelf break the rosette was lowered to less than 2 m above the bottom, and the data were pressure averaged to a resolution of 1 dbar. Gridded fields of the hydrographic variables were constructed for each section using Laplacian-spline interpolation, with a grid spacing of 1–2 km in the horizontal and 5 m in the vertical directions. The basic fields were potential temperature (θ), salinity (S), and potential density referenced to the sea surface (σ_θ). The bottom topography was measured using a 12-kHz Knudsen unit.

b. Velocity

Because absolute velocity information in the Irminger Sea boundary current system is relatively rare, especially in the vicinity of the shelf break, high priority was placed on the collection and processing of the vessel-mounted ADCP data.

1) ADCP DATA COLLECTION AND PROCESSING

R/V *Oceanus* was equipped with a hull-mounted RD Instruments 150-kHz narrow-band ADCP for measuring ship relative velocities. For this cruise the instrument was configured to collect 64 8-m bins. Accounting

² Rudels et al. (1999, 2002) surmised that such a current should exist, but their hydrographic measurements were of insufficient resolution to capture the phenomenon.

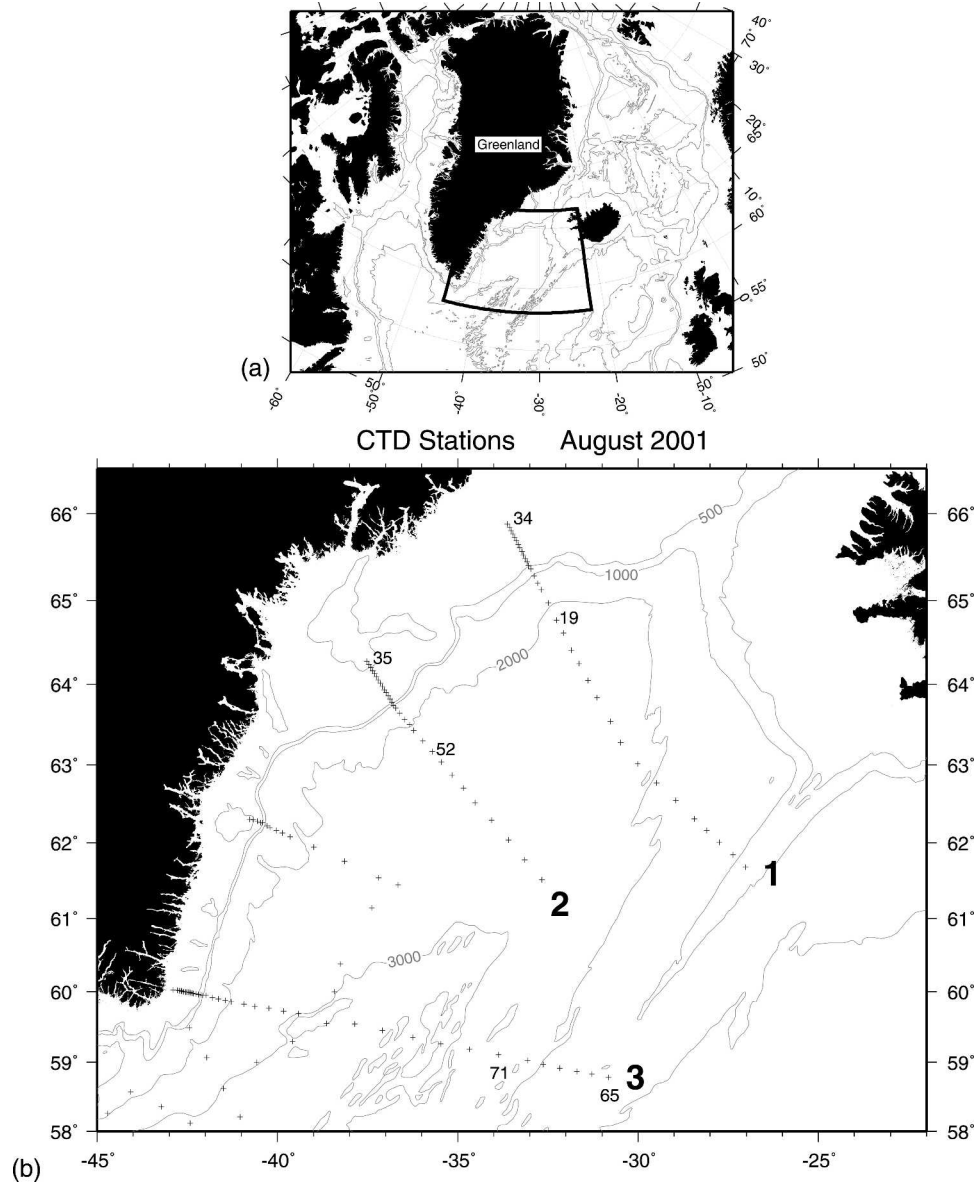


FIG. 2. (a) Study area in the Irminger Sea. (b) The hydrographic survey in summer 2001. CTD stations are marked by the crosses. Section numbers are labeled in boldface lettering, and selected station numbers are indicated in smaller lettering. The bathymetric contours are 500, 1000, 2000, and 3000 m.

for blanking near the surface and the hull depth, the center of the first bin was 17 m. The software used for data collection integrated the GPS data, gyro data, and PC clock information (no Ashtech heading correction was available). Following collection of the data, the Common Ocean Data Access System (CODAS) software package was used for converting the ship relative velocities into absolute velocities. Next, a series of semiautomated programs were used to edit bad points and profiles individually from the dataset. Once these data were removed, calibration calculations were redone to determine if our initial transducer misalignment angle was correct. The amplitude and phase cor-

rections were found to be 0.999° and -0.0087° , which meant no further calibration was necessary.

2) ADCP DE-TIDING

In an effort to remove the barotropic tidal component from the ADCP velocities, we used the Oregon State University (OSU) Ocean Topography Experiment (TOPEX)/Poseidon Cross-Over Global Inverse Solution (Egbert et al. 1994). The version implemented was the $1/2^\circ$ North Atlantic model, which solved for the eight tidal constituents M_2 , S_2 , N_2 , K_2 , K_1 , O_1 , P_1 , and Q_1 . The model was evaluated at each time/location associated with the 5-min ensemble ADCP profiles. Com-

parisons of tidal velocities derived from the OSU model and those calculated from harmonic analysis of moored ADCP data have generally shown good agreement in the western North Atlantic (Torres and Mauritzen 2002). Nonetheless, because of the complex bathymetry of the East Greenland shelf and slope, we compared the Smith and Sandwell bathymetry used in the model with the Knudsen data collected on the cruise and found significant differences in a few regions (mainly around Cape Farewell). An interpolation method was developed for recalculating the tidal correction in the areas where the bathymetry was inaccurate.

3) STREAM COORDINATE ROTATION

After the de-tiding was complete, the ADCP profiles were rotated into a streamwise coordinate system following the methods of Fratantoni et al. (2001). The approach is designed to ensure that comparisons between ADCP velocity sections along the path of the boundary current are not biased by changes in the current's orientation relative to the survey lines. In the rotated coordinate system, the major axis is aligned parallel to the downstream direction of the dominant upper-layer flow. The along-stream direction was defined by the mean transport vector calculated over the upper 250 m of the water column (encompassing the largest velocities in the vicinity of the shelf break) and averaged over the e -folding width of the current. In this approach, we assume that the structure of the current remains largely the same over the along-stream distance sampled in a single section. This distance, and hence the error, is dependent on the width of the current and the angle at which it intersects the survey line. In the two ADCP sections considered here (sections 1 and 2), the survey lines were oriented nearly perpendicular to the dominant flow; hence any error associated with this assumption is small.

4) ABSOLUTE GEOSTROPHIC VELOCITY

To investigate the flow in the deeper part of the water column (i.e., deeper than the penetration depth of the vessel-mounted ADCP) we computed geostrophic velocities and referenced them using the de-tided, stream-coordinate ADCP data. This was done as follows. First the gridded vertical sections of temperature and salinity were used to calculate the dynamic height from which the relative geostrophic velocity was computed. This was then regridded onto the standard grid along with the ADCP along-stream velocity. The former was then referenced by matching the vertically averaged velocity over the depth range of the ADCP data at each horizontal grid location. Although the ADCP velocity field contains ageostrophic contributions (other than the barotropic tide which was removed), these contributions are generally small in comparison with the boundary current flow. This can be seen by noting the good agreement between the vessel-

mounted ADCP velocity and the absolute geostrophic velocity (see next section). We define x , u as the along-stream distance, velocity (positive for shallow water on the right), and y , v as the cross-stream distance, velocity (positive offshore). The depth z is defined as positive upward.

3. Components of the Irminger Sea boundary current system

a. Upper layer

As schematicized in Fig. 1, the cold East Greenland current flows southward through Denmark Strait and meets the warm, retroflected branch of the Irminger Current. This results in a sharp hydrographic front near the shelf break, separating the cold, fresh shelf water from the warm, salty slope water. This front occurs between stations 23 and 24 on our first crossing (Figs. 3a,b). Note that there is a lens of warm, salty slope water located on the shelf inshore of the main front. A similar lens was found on the second hydrographic section (not shown). This is not unexpected since the meandering of this front and the formation of such lenses has long been documented (e.g., Defant 1930; Dietrich 1957a,b; Blindheim 1968; Lee 1968a).

Coincident with the hydrographic front is a sharp change in isopycnal slope, with density surfaces descending as much as 250 m from the outer shelf to the upper slope. This feature has been discussed previously and is thought to be the manifestation of dense water cascading over the shelf break (Rudels et al. 1999; Rudels et al. 2002). Such a process has been documented at numerous other locations around the World Ocean (Ivanov et al. 2004). Rudels et al. (1999) surmised that off of east Greenland this resulted in a shallower, lighter version of the Denmark Strait overflow water flowing southward (perhaps at times merging with the deep overflow). Rudels et al. (2002) reiterated this and speculated that the upper core underwent more intense entrainment than the dense overflow passing through the strait. Neither of these studies had fine enough station spacing to resolve the feature fully, and there was no direct velocity information. Our more detailed dataset verifies the assertions of Rudels et al. (1999; 2002) and documents the existence of this upper core, which we call the East Greenland Spill Jet. Interestingly, Malmberg et al. (1967) noted increased southward flow with depth at the outer shelf in this region, which was likely the same feature.

The vertical section of de-tided velocity from the vessel-mounted ADCP clearly reveals the spill jet (Fig. 4a). One sees the enhanced equatorward flow, greater than 60 cm s^{-1} , banked against the upper continental slope. The absolute geostrophic velocity, referenced using the ADCP data (Fig. 4b), shows the relationship of the spill jet to the East Greenland/Irminger current. The strongest velocities in the latter are associated with

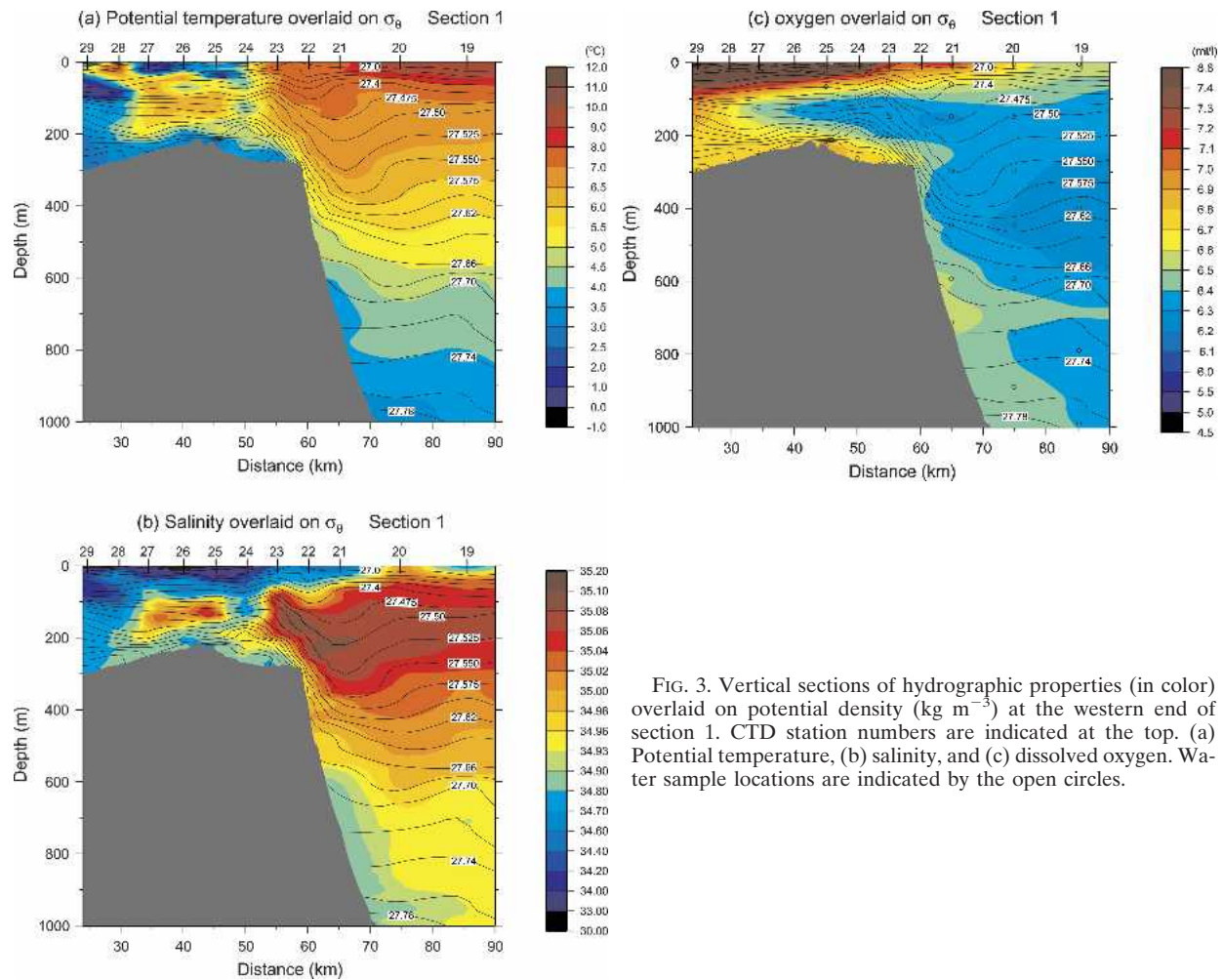


FIG. 3. Vertical sections of hydrographic properties (in color) overlaid on potential density (kg m^{-3}) at the western end of section 1. CTD station numbers are indicated at the top. (a) Potential temperature, (b) salinity, and (c) dissolved oxygen. Water sample locations are indicated by the open circles.

the warm Irminger water, located shallower and offshore of the spill jet. At this northern location, the retro-reflecting Irminger Current is still in the process of merging with the East Greenland Current. Although it is common to depict these two flows side by side along the entire shelf break (as in Fig. 1 and many other schematics), the two are not separable in terms of velocity, which is why we refer to the composite feature as the East Greenland/Irminger Current. Farther downstream the merged velocity signal is located closer to the shelf break.

Note that the spill jet extends from the outer shelf to the upper slope, almost to 1000 m (Fig. 4b). However, the property sections (Fig. 3) show an isolated core of cold, fresh, newly ventilated water confined to the slope near 600–800 m. Did this anomalous water emanate from the shelf, as we assert, or is it instead simply the top of the Denmark Strait overflow core? To shed light on this we computed the vertical section of Richardson number, $R = [N(x, z)/u_z(x, z)]^2$, using the gridded fields of buoyancy frequency (N) and along-stream velocity (u). This reveals an area of small R near the shelf break

and upper slope, which suggests that strong vertical mixing is taking place at that location (Fig. 5). Our interpretation is that entrainment with ambient slope water is occurring as the dense water first spills over the shelf and that this modifies the properties of the shelf water, making it warmer, saltier, and lower in oxygen. By contrast, we surmise that the deeper portion of the spill jet, where the stratification is weaker, did not entrain as rigorously where it spilled over farther upstream. This would explain why the lower portion of the spill jet has more shelflike properties as seen in Fig. 3. A similar contrast in properties is found between the upper and lower portions of the Denmark Strait overflow at the base of the continental slope (see below).

To demonstrate further that turbulent mixing is taking place near the shelf break, we considered individual vertical profiles of N and u . This was motivated by the fact that a certain amount of smoothing occurs when constructing the gridded fields so that the vertical section of R in Fig. 5 is, in fact, a low-passed view. The raw vertical profiles of velocity (from the vessel-mounted ADCP) and buoyancy frequency squared (from the

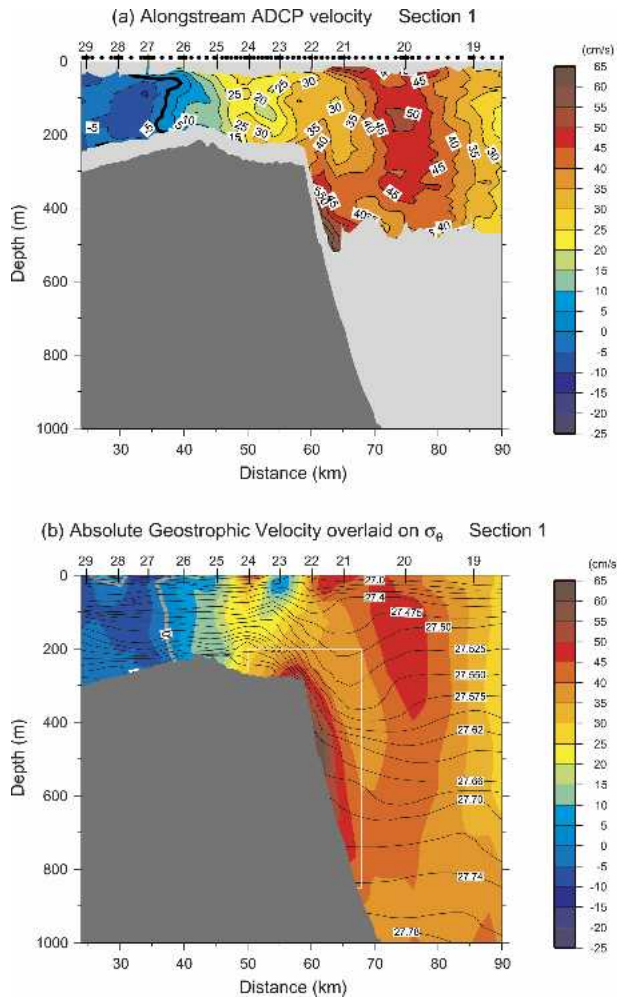


FIG. 4. (a) Along-stream velocity from the vessel-mounted ADCP at the western end of section 1. Positive velocities are equatorward. The area not sampled by the ADCP is blanked by gray shading. CTD station numbers are indicated at the top, and the cross-stream locations of the ADCP ensemble bins are denoted by black circles. (b) Absolute geostrophic velocity referenced using the information in (a) (see text), overlaid on potential density (kg m^{-3}). The thick gray line is the zero velocity contour. The white rectangle is the region used to calculate the volume transport of the spill jet.

CTD) are shown in Figs. 6a and 6b for the site closest to the shelf break. One sees that there is elevated vertical shear in the velocity deeper than 200 m (i.e., the spill jet), which is accompanied by small values of stratification. Together, these result in local values of the Richardson number that fall below the critical value of 1/4 (Fig. 6c), indicating that turbulent entrainment is indeed active in the upper portion of the spill jet.

b. Deep layer

A full water-column view of the along-stream velocity (Fig. 7a) reveals the complete Irminger Sea boundary current system (minus the East Greenland Coastal

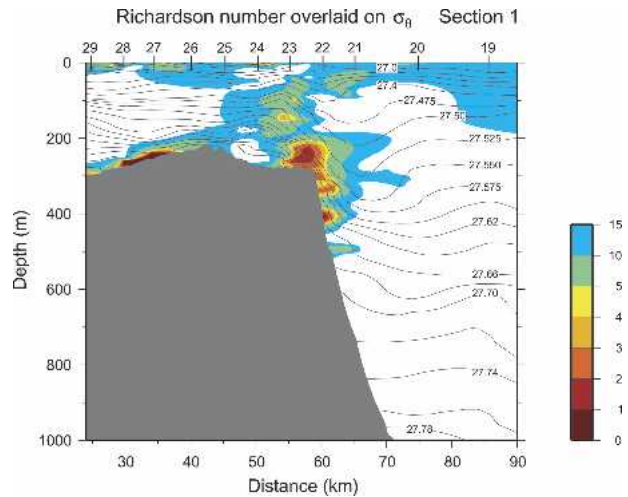


FIG. 5. Vertical section of Richardson number (color) overlaid on potential density (kg m^{-3}) at the western end of section 1.

Current). Beneath the East Greenland/Irminger Current and the spill jet is the bottom-intensified flow of Denmark Strait overflow water. One sees that the core of highest velocity is situated near 1400-m depth, flowing greater than 55 cm s^{-1} . A broad region of weaker flow extends offshore down to the base of the continental slope. The vertical section of oxygen (Fig. 7b) shows that this long tail contains the highest oxygen concentrations, whereas the high-speed core has a markedly reduced signal. This is analogous to the spill jet in that the greatest entrainment—and hence the strongest modification of properties—occurs in the swiftest part of the jet, while the denser, slower component contains the purest form of the water mass.

We note that, in terms of velocity, there is not a huge distinction between the base of the upper-layer components of flow (the spill jet and the East Greenland/Irminger Current) and the top of the overflow. The velocity minimum separating these components is greater than 35 cm s^{-1} . Also note the strong lateral shear in velocity at the edge of the composite boundary current, near station 18. This shear would not have been evident from the thermal wind alone, and further demonstrates the importance of the vessel-mounted ADCP data in referencing the geostrophic velocity. The isopycnal that separates the upper-shelfbreak system from the deeper Denmark Strait overflow water is $\sigma_\theta = 27.76 \text{ kg m}^{-3}$. This is smaller than the value typically used to delineate the overflow (27.8 kg m^{-3} ; see Dickson and Brown 1994) and may be a reflection of interannual variability (e.g., Bacon 1998).

4. Transports

Despite the fact that there have been numerous surveys of the western Irminger Sea boundary current system over the years, very few absolute transport esti-

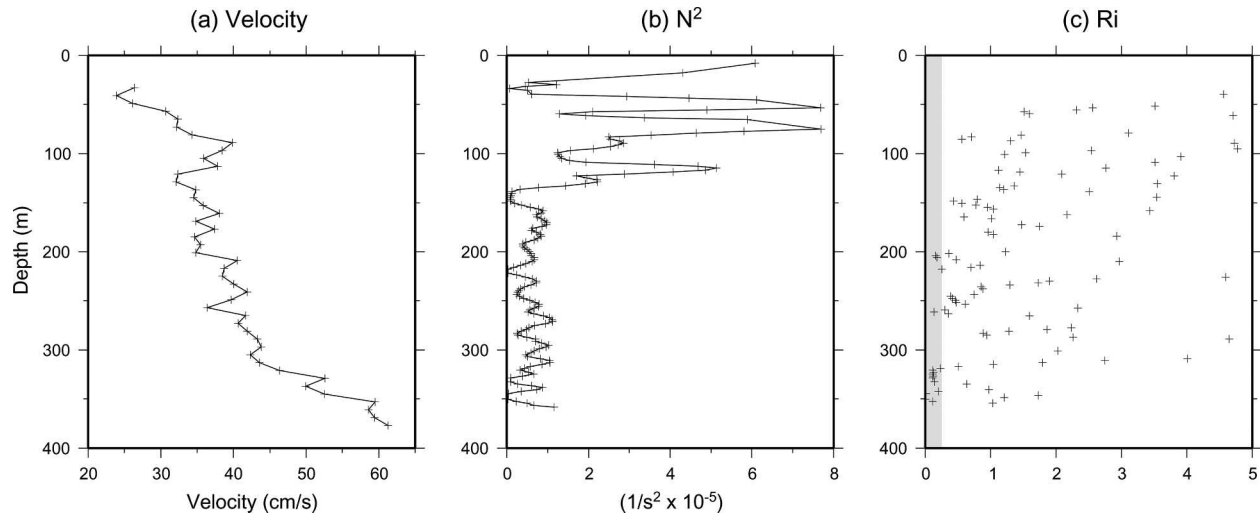


FIG. 6. (a) Unsmoothed ADCP along-stream velocity profile at the bin location closest to CTD station 22. Positive velocities are equatorward. (b) Vertical profile of buoyancy frequency squared at CTD station 22 (the data have been subsampled for presentation). (c) Richardson number calculated from (a) and (b). The gray shading denotes values less than the critical number of $1/4$.

mates exist because there is a lack of direct velocity measurements. One notable exception is the study by Clarke (1984), who used current-meter data from short-term deployments to reference a hydrographic section off of Cape Farewell (the offshore part of the section was referenced subjectively, however). A second exception is the investigation of Dickson and Brown (1994), who presented a rigorous calculation of the downstream evolution in transport of the Denmark Strait overflow layer (although the East Greenland/Irminger Current was not sampled by the current-meter arrays). Our survey offers the best opportunity to date in terms of lateral coverage (with absolute velocity), but one needs to keep in mind that this is a synoptic snapshot, subject to inherent mesoscale variability.

Some of the historical transport calculations consider the East Greenland/Irminger current as a single entity (e.g., Bacon 1997), while others resolve the two components (e.g., Dietrich et al. 1980). To separate the two parts it is necessary to define a watermass boundary between the East Greenland Current water and the Irminger Water, which is not straightforward. For example, both Blindheim (1968) and Clarke (1984) used the 34.5 isohaline as the boundary, but in some of Blindheim's sections this is closer to the dividing line between the East Greenland Current and the East Greenland Coastal Current. This is true for our realization as well. Clearly this division is subject to interannual variability, and for our 2001 data we chose $S = 34.9$ psu as the dividing isohaline between the cold, fresh East Greenland Current water and the warm, salty Irminger Current water (see Fig. 3b). As for the other components of the flow, the chosen limits of the spill jet are shown in Fig. 4, and, as noted above, the layer from $\sigma_\theta = 27.76 \text{ kg m}^{-3}$ to the bottom is taken as the Denmark Strait overflow water.

Two of the hydrographic sections in our survey extended to the Reykjanes Ridge (Fig. 2), and on both sections we sampled the northward-flowing Irminger Current situated over the western flank of the ridge. This was evident both in the vessel-mounted ADCP data and in the hydrography (a transition into saltier water over the ridge). At the northern section the ADCP velocity vectors indicate that the current was heading north-northwestward, and hence we crossed it at an oblique angle. For this reason we used the southern crossing to compute the northward transport of the current. Figure 8 shows this cross section of the current, which has a similar structure to the Gulf Stream from which it derives—albeit smaller and weaker. A pronounced salinity front shows the transition to subtropical waters, and the associated density front supports a current that is greater than 40 cm s^{-1} . For the transport we used $\sigma_\theta = 27.76 \text{ kg m}^{-3}$ as the lower boundary of the flow (to be consistent with the western boundary), and the lateral domain was taken to be 530–605 km (Fig. 8).

A geographical view of the transport distribution of the boundary current system is shown in Fig. 9a. In the figure the directly computed transport values appear in the yellow squares. It is seen that the East Greenland portion of the combined East Greenland/Irminger Current is 0.7 Sv ($\text{Sv} \equiv 10^6 \text{ m}^3 \text{ s}^{-1}$), while the Irminger portion is 12.9 Sv. Note that the latter includes the spill jet, which is 1.9 Sv. Farther to the south we were able to cross the East Greenland Coastal Current (near Cape Farewell, where ice was not a problem), which is transporting 2.0 Sv. We have no direct measure of the Icelandic Irminger Current flowing northward into the Iceland Sea nor have we measured the cold outflow of the East Greenland Current prior to joining the Irminger Current. To put our synoptic transport scheme into context with the transport budget of the Nordic seas as

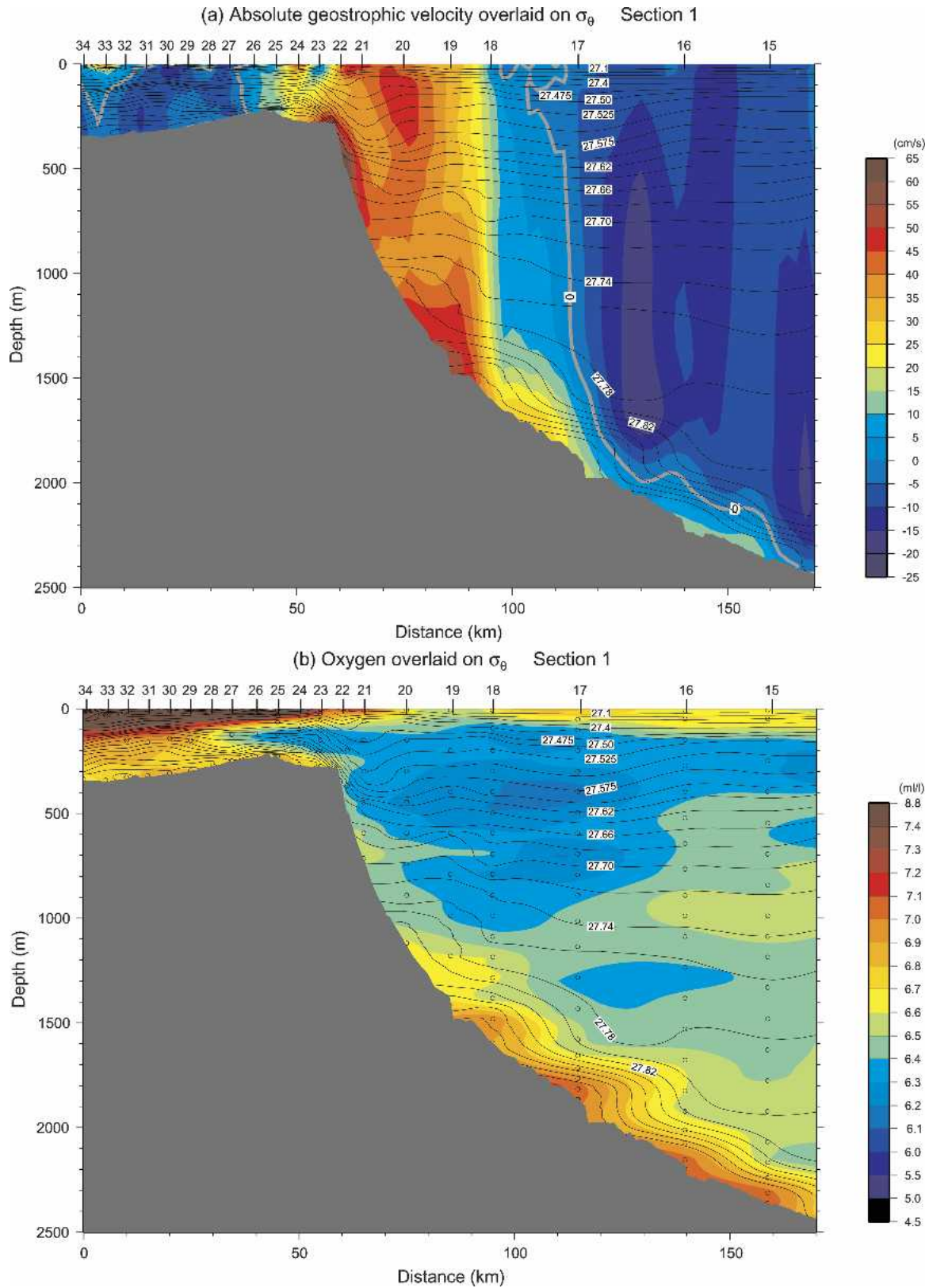


FIG. 7. Full-water column vertical sections. (a) Absolute geostrophic velocity (color) overlaid on potential density (kg m^{-3}) at the western end of section 1. Positive velocities are equatorward. The thick gray line is the zero velocity contour. (b) Dissolved oxygen (color) overlaid on potential density. Water sample locations are indicated by the open circles.

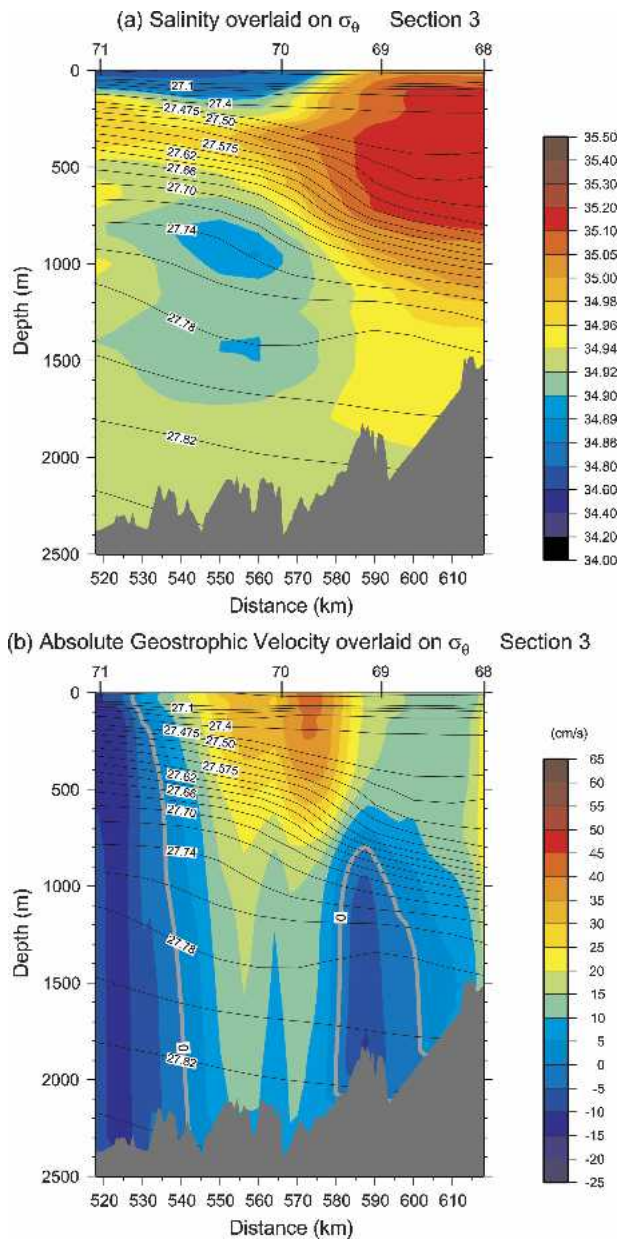


FIG. 8. (a) Salinity (color) overlaid on potential density (kg m^{-3}) at the eastern end of section 3, over the western flank of the Reykjanes Ridge. (b) Absolute geostrophic velocity (color) overlaid on potential density. Positive velocities are poleward. The thick gray line is the zero velocity contour.

a whole, it is desirable to estimate these values. We do so as follows.

Figure 10 shows the Nordic seas transport budget from Hansen and Osterhus (2000), which they argue is accurate to within 1 Sv. In their scheme, 7 Sv of Atlantic water enter the basin in the east and 1 Sv enters in the west, comprising the Icelandic Irminger Current. If we take this value for the Icelandic Irminger Current in our survey, it means that 12.7 Sv of the northward-flowing

Irminger Current recirculates south of Denmark Strait. This in turn implies that the spill jet would consist of nearly all recirculated Atlantic water, which is clearly not the case. In the other extreme, if we assume 3 Sv of water flow northward in the Icelandic Irminger Current, this implies that no recirculated Irminger Current water would be in the spill jet, which is also unlikely. We therefore assign an intermediate value of 2 Sv to the Icelandic Irminger Current. For the East Greenland Current emanating from the Iceland Sea we have no compelling reason not to use the value of 1.3 Sv quoted by Hansen and Osterhus (2000). This in turn implies that in our scheme the spill jet is composed of roughly 0.7 Sv of recirculating Irminger Current water, 0.6 Sv of pure East Greenland Current water, and 0.6 Sv due to entrainment of additional ambient water adjacent to the shelf. While this scenario is of course speculative, it is nonetheless plausible in light of the evidence presented above for significant entrainment at the shelf break as the spill jet forms. It is also consistent with the temperature–salinity distribution of the water comprising the spill jet, which is shown in Fig. 11. One sees a spread of T – S values ranging from the extreme of East Greenland Current water to the opposite extreme of pure Irminger water.

Our estimated values of inflow and outflow from the Iceland Sea are included in Fig. 9a (shown in cyan circles, since they are not directly calculated), which then gives a complete scheme for the transport of the Irminger Sea boundary current system. These transport estimates are compared with historically calculated values in Fig. 9b, and also listed in Table 1. Summarizing our scheme, nearly 14 Sv of warm, salty Irminger water approaches Denmark Strait from the south, and roughly 85% of this retroflects to the southwest. Our value of 2 Sv for the Icelandic Irminger Current is somewhat large (although it falls within the range of values presented in Table 1), but one should keep in mind that the degree of retroflexion is thought to vary in time. For example, one of the influencing factors is the local winds (Steffansson 1962; Blindheim 1968), which can enhance the Atlantic inflow when blowing from the south. Regarding the cold outflow, the East Greenland Current is transporting 1.3 Sv of water out of Denmark Strait. Nearly half of this cascades over the shelf and entrains ambient water—including some of the retroflected Irminger Current water—to form the spill jet carrying 1.9 Sv. We also calculate 2 Sv for the East Greenland Coastal Current on the inner shelf, which is significantly larger than Bacon et al.'s (2002) estimate at the same location (0.8 Sv).³ Regarding the deep flow, the transport of Denmark Strait overflow

³ We note that Bacon et al. (2002) show drifter-derived surface currents $>100 \text{ cm s}^{-1}$ in the East Greenland Coastal current, suggesting a greater transport than that derived from their ADCP data.

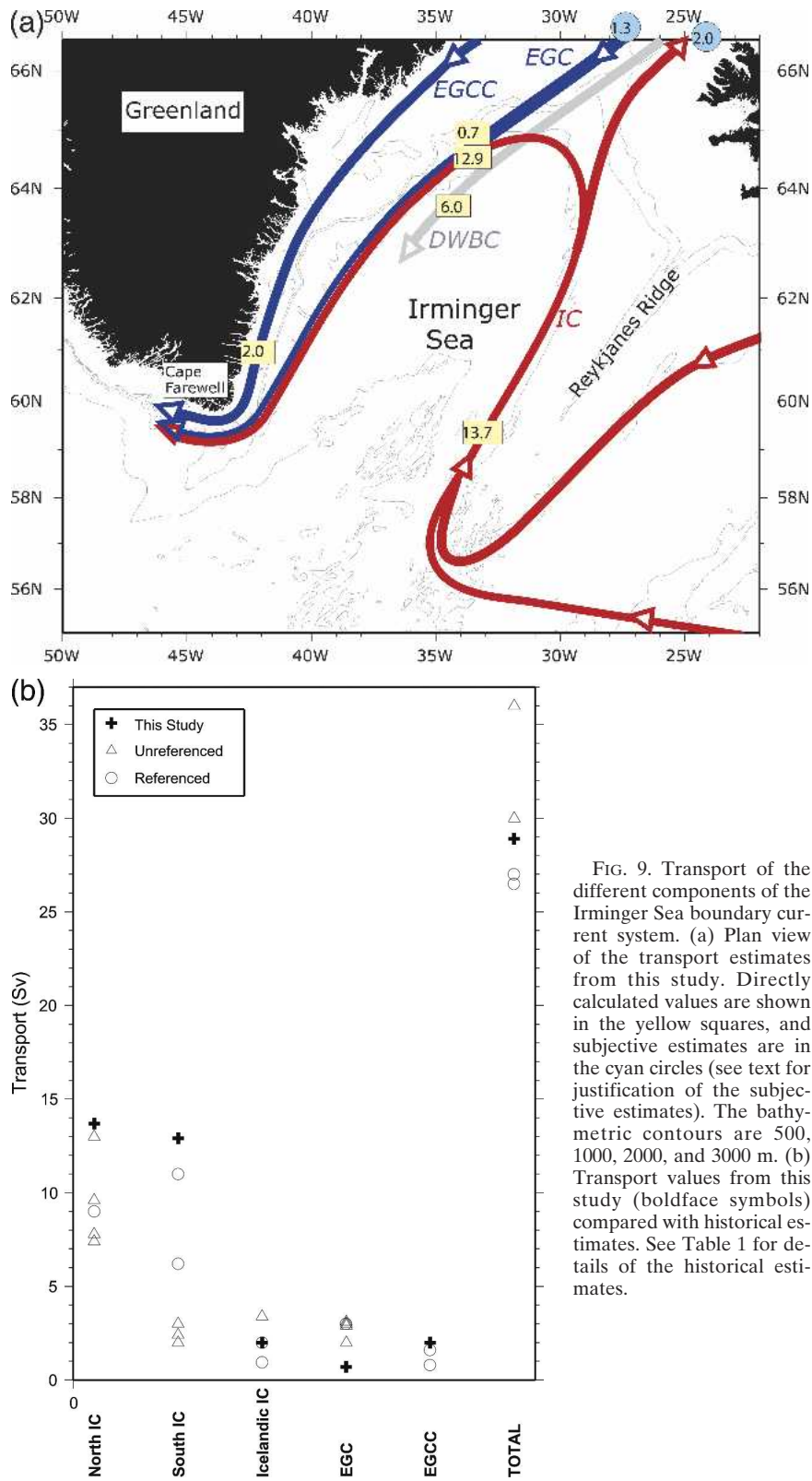


FIG. 9. Transport of the different components of the Irminger Sea boundary current system. (a) Plan view of the transport estimates from this study. Directly calculated values are shown in the yellow squares, and subjective estimates are in the cyan circles (see text for justification of the subjective estimates). The bathymetric contours are 500, 1000, 2000, and 3000 m. (b) Transport values from this study (boldface symbols) compared with historical estimates. See Table 1 for details of the historical estimates.

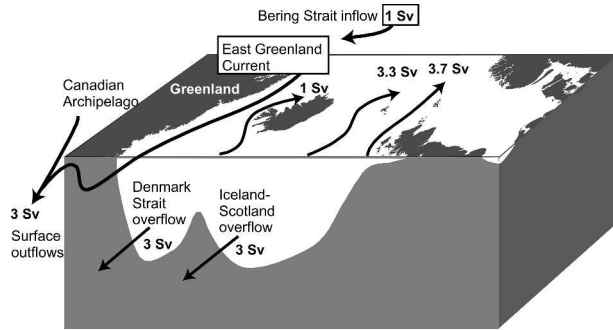


FIG. 10. Schematic of the water balance in the Nordic seas, from Hansen and Osterhus (2000).

water at section 1 is 6.0 Sv, in line with what Dickson and Brown (1994) present for this location (5.2 Sv).

Does our synoptic scheme make sense in terms of the overall balance for the Nordic seas? Comparing Figs. 9a and 10 it is seen that we have more warm inflow (1 Sv more) as well as more cold surface outflow (2 Sv more) than in the budget presented by Hansen and Osterhus (2000) (we assume that the deep outflows and the eastern Atlantic inflow are the same in both schemes, along with the Bering Strait and Canadian Arctic Archipelago contributions). This difference could be due to the fact that our scheme is an instantaneous snapshot, whereas Hansen and Osterhus' (2000) budget is based on long-term measurements. Nonetheless, our scheme balances the Nordic seas inflow/outflow to within 1 Sv, which is the uncertainty quoted by Hansen and Osterhus (2000). The imbalance of excess outflow in Fig. 9a becomes smaller when one considers that some of the

East Greenland Coastal Current at Cape Farewell is likely due to runoff emanating from south of Denmark Strait. In any event, even though our survey is synoptic, it suggests that a significant amount of the cold, fresh outflow of the Nordic seas occurs in the East Greenland Coastal Current.

Last, we address the total western boundary current transport exiting the Irminger Sea to the south. As depicted in Dickson and Brown (1994), the deep-layer transport increases downstream of Denmark Strait, primarily because of the addition of the Iceland–Scotland overflow water from the Gibbs Fracture Zone. If we assume the same enhancement to the south, which increases the deep transport to 13.3 Sv at Cape Farewell, and assume that the spill jet does not increase its transport significantly further (see below), this gives a total equatorward volume flux of 28.9 Sv at 60°N. This is fairly close to the other directly referenced estimates at this location—Clarke's (1984) range of 27–33 Sv and Bacon's (1997) value of 26–27 Sv based on inverse constraints. It is also in line with the mean estimate of 28.5 Sv that Pickart and Spall (2004) obtained for the northward-directed total transport on the west side of Greenland (at the WOCE AR7W line). This latter agreement may be fortuitous, however. The Lagrangian results of Lavender et al. (2000) and others have suggested that there are local deep recirculations in both the Irminger and Labrador Seas. Pickart and Spall's (2004) estimate excludes the recirculating component, whereas our Irminger Sea calculation (and that of Clarke 1984 and Bacon 1997) does not attempt to separate throughput from recirculation. Furthermore, Pickart and Spall's (2004) mean section does not include the full contribution from the West Greenland Current. More refinement will be required to pin down the precise boundary current throughput in this region of the subpolar gyre.

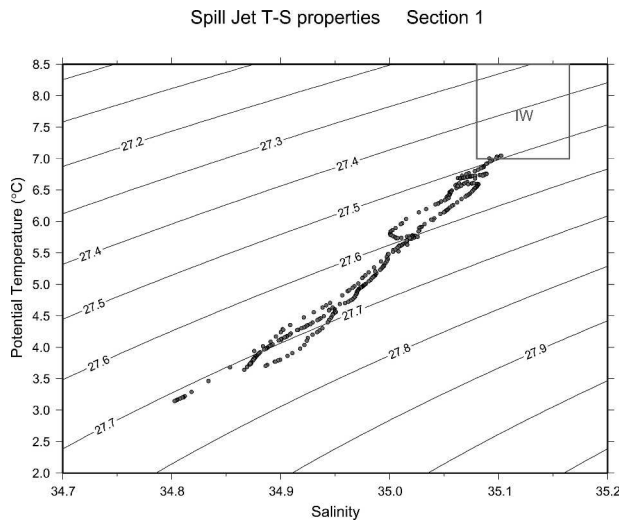


FIG. 11. The T - S scatterplot for the water comprising the spill jet, computed from those parts of stations 21–24 that fall within the white box shown in Fig. 4b; IW denotes the Irminger Water end member, whose bounds were computed from stations 68–69 using data between 100 and 600 m (Fig. 8).

5. Vorticity structure of the spill jet

To understand better the character of the spill jet and the possible nature of its spatial and temporal variability, we considered the cross-stream structure in vorticity. In particular, we constructed vertical sections of the different components of the Ertel potential vorticity,

$$\Pi = \frac{-f \partial \sigma_{\theta}}{\rho_0 \partial z} + \frac{1}{\rho_0} \frac{\partial u}{\partial y} \frac{\partial \sigma_{\theta}}{\partial z} - \frac{g}{\rho_0^2 f} \left(\frac{\partial \sigma_{\theta}}{\partial y} \right)^2, \quad (1)$$

where f is the (constant) Coriolis parameter ($1.31 \times 10^{-4} \text{ s}^{-1}$), ρ_0 is the reference density ($1.031 \times 10^3 \text{ kg m}^{-3}$), and g is the gravitational acceleration. The first term on the right-hand side of (1) is the vertical stretching term, while the second term is the relative vorticity, which is dominated by the cross-stream shear in equatorward velocity. The third term is a nonquasi-geostrophic contribution to the vorticity known as the tilting term [see Hall (1994) for a derivation of this term]. In large-scale relatively weak flows, the stretch-

TABLE 1. Historical transport estimates (Sv) of the Irminger Sea boundary current system.

Study	Northward-flowing Irminger Current	Southward-flowing Irminger Current	Icelandic Irminger Current	East Greenland Current	Combined East Greenland and southward-flowing Irminger Current	East Greenland Coastal Current	Total western boundary current off southern Greenland	Absolute reference	Comment
Lee (1968a)		3.0	2.9				No	Average of International Ice Patrol repeat hydrography from 1950–63.	
Dietrich (1957b)	7.4		3.0				No		
Worthington (1970)			3.0				No		
Malmberg et al. (1967)					1.6		Yes	Referenced using moorings.	
Lee (1968b)	7.8	2.4					No	Relative to 1000 m. NORWESTLANT 2.	
Dietrich et al. (1980)		2.0	2.0				No		
Clarke (1984)		11.0	3.0			27–33.5	Yes	Shoreward part of section referenced using short-term moorings.	
Reid (1994)						3.0	No		
Schmitz and McCartney (1993)						36	No		
Krauss (1995)	9.6	6.2	3.4				Yes/no	Only the southward-flowing Irminger current value is referenced using float data. The Icelandic Irminger current estimate is a residual.	
Bacon (1997)	9.0				15.0	26–27	Yes	Referenced using vessel-mounted ADCP, inverse calculation.	
Bacon et al. (2002)							No	Calculated using hydrography and model.	
Jonsson and Briem (2003)			0.95			0.8	Yes	Calculated using long-term moorings.	
S. Jonsson (2004, personal communication)			2				Yes	Calculated using vessel-mounted ADCP data.	
Pollard et al. (2004)	9.0–13.0				7.0		No	Relative to 1400 m or bottom.	
This study	13.7	12.9	2.0	0.7	13.6	2.0	Yes	The Icelandic Irminger current value is subjective; all other values are directly calculated. The total transport value assumes enhancement of deep layer transport according to Clarke (1984; see text).	

ing term dominates Π (e.g., Talley and McCartney 1982), but in strong jets like the Gulf Stream all three terms can contribute (Hall 1994). The tilting vorticity becomes significant in regions of strongly sloped isopycnals, so we would expect this term to be important in the spill jet because of the strong density front at the shelf break (Fig. 3).

The ratio of the relative vorticity and the tilting vorticity to the stretching term (Fig. 12) reveals that all three components of Π are significant in the spill jet. Strong cyclonic vorticity, exceeding $0.5f$, is found adjacent to the upper slope (Fig. 12a). This suggests that the current may be barotropically unstable. This has recently been purported for the boundary current on the west side of Greenland because of the strong lateral velocity shear adjacent to the boundary (Eden and Böning 2002), as well as for various other boundary current systems around the World Ocean (e.g., in the western Arctic shelfbreak jet; Paquette and Bourke

1974). The relative vorticity is likely even stronger in the narrow spill jet than it is on the west side of Greenland. The tilting vorticity is also strong in the spill jet, greater than $0.4f$ in the vicinity of the shelf break (Fig. 12b).

To elucidate further the cross-stream vorticity structure we computed a depth-layer average (300–500 m) of the terms in Π , which is displayed in Fig. 13. The region of the spill jet is shaded in the figure, and one sees that the cyclonic relative vorticity increases markedly toward the boundary. Note however that, since the tilting vorticity has the opposite trend, these two terms partially cancel each other. The net effect on Π is to sharpen the transition from a low value of potential vorticity offshore to a high, generally uniform value in the spill jet. Such a potential vorticity front is reminis-

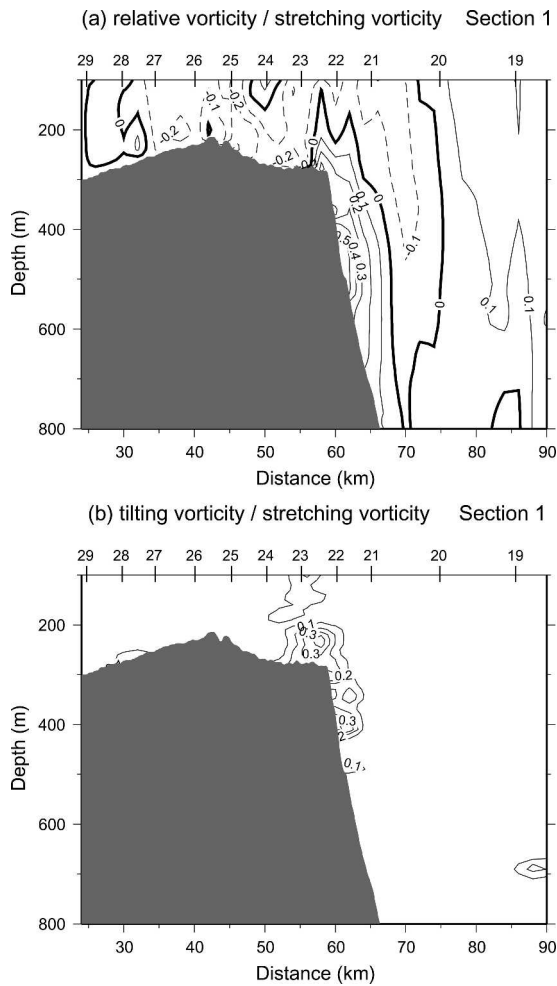


FIG. 12. (a) Vertical section of the ratio of relative vorticity to stretching vorticity [see Eq. (1)] at the western end of section 1. Solid contours are cyclonic vorticity, and dashed contours are anticyclonic. (b) Ratio of tilting vorticity to stretching vorticity.

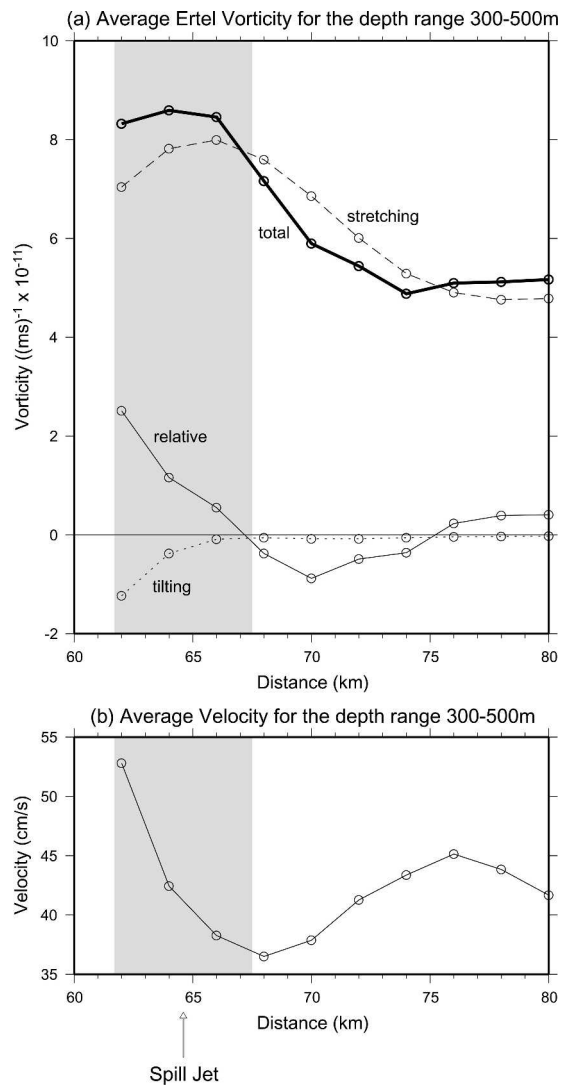


FIG. 13. (a) Terms of the Ertel vorticity at the western end of section 1, averaged over the depth layer 300–500 m. The shaded region denotes the spill jet. (b) Average along-stream velocity in the same depth layer.

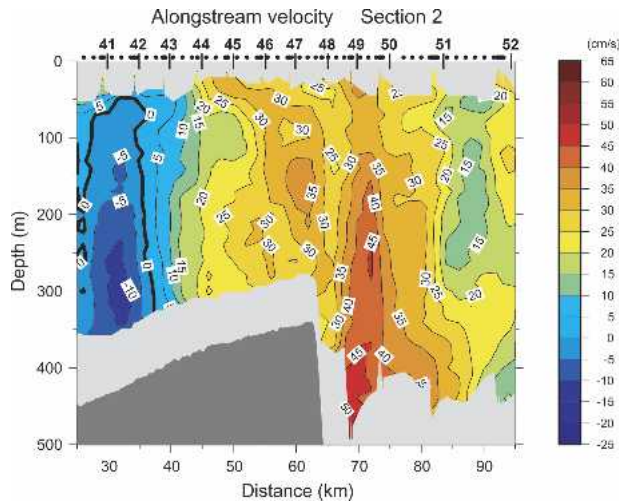


FIG. 14. Along-stream velocity from the vessel-mounted ADCP at the western end of section 2. Positive velocities are equatorward. See caption to Fig. 4a for other details of the plot.

cent of the Gulf Stream (Hall 1985) and is believed to influence the turbulent behavior of that current. Pratt and Stern (1986) modeled a jet, located adjacent to a sidewall, with this same potential vorticity structure. They found that meanders in the current's path developed at finite amplitude, and eddies were subsequently formed. This could be happening in the spill jet as well, whereby an initial disturbance (resulting say from barotropic instability) would grow to finite amplitude and ultimately lead to cross-frontal exchange. This is intriguing because it suggests that the process of transferring dense water from the shelf to the interior basin may involve two steps: First, the spilling process forms the intense jet flowing along the upper slope, then the unstable character of the jet leads to lateral exchange of mass and properties.

6. Discussion

While our measurements have offered a first glimpse of the nature, transport, and structure of the East Greenland Spill Jet, a host of issues remain to be sorted out. These include determining the formation mechanism, the seasonality, and the fate of the jet, as well as its role in shelf–basin exchange in the Irminger Sea. Some of these issues can be addressed with future field programs, while some will require high-resolution modeling. Using our present dataset we can make a few general statements, and a few speculations.

The spill jet was observed as well at the next two hydrographic sections south of our northern line. This can be seen in the vessel-mounted ADCP along-stream velocity sections (Fig. 14). On the outer shelf and upper slope (shallower than the shelf break) one sees the signal of the East Greenland/Irminger Current, which is now more fully merged in the vicinity of the shelf break.

Deeper than this the equatorward velocity again increases with values greater than 50 cm s^{-1} adjacent to the continental slope. This is clearly the spill jet. Using the section of absolute geostrophic velocity referenced with the ADCP data (not shown), we calculate a transport of 2.4 Sv. The similarity of this value to the transport computed upstream suggests that further entrainment by the spill jet is minimal as it flows equatorward. This is in contrast to the deeper Denmark Strait overflow, which nearly doubles its transport south of the strait (Dickson and Brown 1994). Hence, near their origins the spill jet and overflow water have similar transports (roughly 2 Sv), but the spill jet apparently does not entrain significantly more water. This is consistent with the hydrography as well, which indicates that the average properties of the spill jet are nearly the same at sections 1 and 2. In particular, for the portion of the jet that has spilled over the shelf break, the difference is only 0.26°C for potential temperature, 0.006 for salinity, and 0.019 kg m^{-3} for potential density. This demonstrates further that entrainment is minimal between the two locations.

What is the ultimate fate of the spill jet? By the latitude of Cape Farewell (section 3 in Fig. 2) it is no longer distinguishable from the East Greenland/Irminger Current. Since this section coincides with the WOCE A1E line, it has been occupied numerous times over the past 15 years (although not at high resolution near the shelf break). Inspection of these sections (plus our 2002 and 2003 high-resolution occupations) reveals that the frontal density structure of the spill jet is not present at 60°N (see Fig. 9 in Pickart et al. 2002). Two possibilities are that the jet somehow merges with the East Greenland/Irminger Current or that it basically disintegrates because of instability (as discussed above). Further work will be necessary to sort this out.

It is of much interest as well to determine why the dense water spills over the shelf in the first place south of Denmark Strait. Here we are left to speculation and anecdotal information. We know from previous studies, and our own measurements, that the East Greenland/Irminger front is unstable in that warm, salty Irminger water is commonly found on the shelf. This was noted in Fig. 3 and was observed even more markedly in our 2003 survey in this region. One is then tempted to invoke baroclinic instability as a means for a two-way exchange across the shelf break, with buoyant water being fluxed onshore in the upper layer and dense water being fluxed offshore near the bottom. Winds could also play a role. One of the dominant wind regimes in this region is the East Greenland barrier winds (Capellen et al. 2001), which flow from the northeast parallel to the Greenland coast. These are downwelling favorable, which is conducive for offshore transport near the bottom across the shelf. Recent work (Thomas and Lee 2005) also shows that such along-current winds can lead to cyclogenesis, which could impact the stability of the current as well.

Last, one wonders about the origin of the dense water in the spill jet. Has it formed locally (and has thus in turn facilitated the spilling) or has it been advected remotely from north of Denmark Strait (as implied in our earlier discussion on transports)? The strong stratification on the shelf in Fig. 3 suggests the latter, but one must keep in mind the strong wintertime buoyancy forcing in this region. The air–sea heat flux due to the barrier winds is quite strong (see Pickart et al. 2003), and brine formation may lead to overturning. Convection near the outer shelf can also be enhanced by surface Ekman flux of dense, salty water from offshore due to the northerly winds (Straneo et al. 2001). On the other hand, there are a variety of water masses being advected southward in the East Greenland Current north of Denmark Strait, which could be supplying the source waters of the spill jet. Inspection of the property sections in Rudels et al. (2002) suggest that the spill jet may be composed of modified Polar Intermediate Water. Clearly, more investigation is needed to begin sorting out this issue, as well as the other spill jet issues raised above. A hydrographic survey completed in summer 2004 was a first step toward this.

Acknowledgments. We are grateful to Captain A. Mello and the crew of the R/V *Oceanus* for their diligent efforts in collecting these data. During the cruise we also received assistance from the Danish Meteorological Institute in the way of weather and ice information. We are especially grateful to E. Buch, M. Ribergaard, and K. Hansen for their help with the field program. The CTD data processing was carried out by T. McKee. D. Sutherland provided one of the figures. We would also like to acknowledge P. Ehrenbrink, who translated several old German articles into English. This project was funded by the National Science Foundation under Grant OCE 00-02492.

REFERENCES

- Bacon, S., 1997: Circulation and fluxes in the North Atlantic between Greenland and Ireland. *J. Phys. Oceanogr.*, **27**, 1420–1435.
- , 1998: Decadal variability in the outflow from the Nordic Seas to the deep Atlantic Ocean. *Nature*, **394**, 871–874.
- , G. Reverdin, I. G. Rigor, and H. M. Snaith, 2002: A freshwater jet on the east Greenland shelf. *J. Geophys. Res.*, **107**, 3068, doi:10.1029/2001JC000935.
- Blindheim, J., 1968: Hydrographic investigations in the Irminger Sea in the years 1954–1964. *FiskDir. Skr. Ser. HavUnders.*, **14**, 72–97.
- Bower, A. S., and Coauthors, 2002: Directly measured mid-depth circulation in the northeastern North Atlantic Ocean. *Nature*, **419**, 603–607.
- Cappelen, J., B. V. Jorgensen, E. V. Laursen, L. S. Stannius, and R. S. Thomsen, 2001: The observed climate of Greenland, 1958–99, with climatological standard normals, 1961–90. Danish Meteorological Institute Tech. Rep. 00–18, 149 pp.
- Clarke, R. A., 1984: Transport through the Cape Farewell–Flemish Cap section. *Rapp. P.-V. Reun.-Cons. Int. Explor. Mer.*, **185**, 120–130.
- Defant, A., 1930: Bericht über die ozeanographischen Untersuchungen des Vermessungsschiffes “Meteor” in der Danemarkstrasse und in der Irmingersee. *Preuss. Akad. Wiss., Sitz., Phys. Math. Klasse*, **XVI**, 230–235.
- , 1936: Bericht über die ozeanographischen Untersuchungen des Vermessungsschiffes “Meteor” in der Danemarkstrasse und in der Irmingersee. *Preuss. Akad. Wiss., Sitz., Phys. Math. Klasse*, **XIX**, 232–242.
- Dickson, R. R., and J. Brown, 1994: The production of North Atlantic deep water: Sources, rates, and pathways. *J. Geophys. Res.*, **99**, 12 319–12 341.
- Dietrich, G., 1957a: Ozeanographische probeme der deutschen Forschungsfahrten im Internationalen Geophysikalischen Jahr 1957/58. *Deutsche Hydrographische Zeitschrift*, **2**, 39–61.
- , 1957b: Schichtung und Zirkulation de Irminger See in Juni 1955. *Berichte der Deutsche Wissenschaftlichen Kommission für Meeresforschung, Neue Folge*, **14**, 255–312.
- , 1964: Oceanic polar front survey in the North Atlantic. *Res. Geophys.*, **2**, 291–308.
- , K. Kalle, W. Krauss, and G. Siedler, 1980: *General Oceanography: An Introduction*. 2d ed. John Wiley and Sons, 626 pp.
- Eden, C., and C. Böning, 2002: Sources of eddy kinetic energy in the Labrador Sea. *J. Phys. Oceanogr.*, **32**, 3346–3363.
- Egbert, G. D., A. F. Bennett, and M. G. G. Foreman, 1994: TOPEX/POSEIDON tides estimated using a global inverse model. *J. Geophys. Res.*, **99**, 24 821–24 852.
- Fiedler, A., 2003: Om Irminger Havets og Irminger Strommens navn. *Sovoersorientering*, **1**, 1–3.
- Fratantoni, D. M., 2001: North Atlantic surface circulation during the 1990’s observed with satellite-tracked drifters. *J. Geophys. Res.*, **106**, 22 067–22 093.
- , R. S. Pickart, D. J. Torres, and A. Scotti, 2001: Mean structure and dynamics of the shelfbreak jet in the Middle Atlantic Bight during fall and winter. *J. Phys. Oceanogr.*, **31**, 2135–2156.
- Hall, M. M., 1985: Horizontal and vertical structure of velocity, potential vorticity, and energy in the Gulf Stream. Ph.D. thesis, Massachusetts Institute of Technology, 165 pp.
- , 1994: Synthesizing the Gulf Stream thermal structure from XBT data. *J. Phys. Oceanogr.*, **24**, 2278–2287.
- Hamberg, A., 1884: Hydrographic observations of the Nordenkiöld Expedition to Greenland, 1883. *Proceedings Royal Society*, London.
- Hansen, B., and S. Osterhus, 2000: North Atlantic–Nordic Seas exchanges. *Progress in Oceanography*, Vol. 45, Pergamon, 109–208.
- Ivanov, V. V., G. I. Shapiro, J. M. Huthnance, D. L. Aleynik, and P. N. Golovin, 2004: Cascades of dense water around the world ocean. *Progress in Oceanography*, Vol. 60, Pergamon, 47–98.
- Jakobsen, P. K., M. H. Ribergaard, D. Quadfasel, T. Schmith, C. W. Hughes, 2003: Near-surface circulation in the northern North Atlantic as inferred from Lagrangian drifters: Variability from the mesoscale to interannual. *J. Geophys. Res.*, **108**, 3251, doi:10.1029/2002JC001554.
- Jonsson, S., and J. Briem, 2003: Flow of Atlantic water west of Iceland and onto the north Icelandic shelf. *ICES Mar. Sci. Symp.*, **219**, 326–328.
- Knudsen, M., 1899: *Hydrography*. Danish *Ingolf* Expedition, Bd. I, No. 2, Copenhagen.
- Krauss, W., 1995: Currents and mixing in the Irminger Sea and in the Iceland Basin. *J. Geophys. Res.*, **100**, 10 851–10 871.
- Lavender, K. L., R. E. Davis, and W. B. Owens, 2000: Mid-depth recirculation observed in the interior Labrador and Irminger Seas by direct velocity measurements. *Nature*, **407**, 66–69.
- Lee, A. J., 1968a: NORWESTLANT Surveys: Physical Oceanography. *ICNAF Special Publication, Environmental Surveys*, Vol. 7, Part I, 31–54.
- , 1968b: NORWESTLANT Surveys: Physical Oceanography.

- ICNAF Special Publication, Environmental Surveys*, Vol. 7, Part II, 38–159.
- Malmberg, S.-A., H. G. Gade, H. E. Sweers, 1967: Report on the second joint Icelandic-Norwegian expedition to the area between Iceland and Greenland in August–September 1965. NATO Subcommittee on Oceanographic Research Tech. Rep. 41, Irminger Sea Project, 44 pp.
- Paquette, R. G., and R. H. Bourke, 1974: Observations on the coastal current of Arctic Alaska. *J. Mar. Res.*, **32**, 195–207.
- Pickart, R. S., and M. A. Spall, 2004: Heat transport in the Labrador Sea. *Geophys. Res. Abs.*, **6**, EGU04-A-03974.
- , D. J. Torres, and R. A. Clarke, 2002: Hydrography of the Labrador Sea during active convection. *J. Phys. Oceanogr.*, **32**, 428–457.
- , F. Straneo, and G. W. K. Moore, 2003: Is Labrador Sea Water formed in the Irminger Basin? *Deep-Sea Res.*, **50A**, 23–52.
- Pollard, R. T., J. F. Read, and N. P. Holliday, 2004: Water masses and circulation pathways through the Iceland Basin during Vivaldi 1996. *J. Geophys. Res.*, **109**, C04004, doi:10.1029/2003JC002067.
- Pratt, L. J., and M. E. Stern, 1986: Dynamics of potential vorticity fronts and eddy detachment. *J. Phys. Oceanogr.*, **16**, 1101–1120.
- Reid, J. L., 1994: On the total geostrophic circulation of the North Atlantic Ocean: Flow patterns, tracers, and transports. *Progress in Oceanography*, Vol. 33, Pergamon, 1–92.
- Reverdin, G., P. P. Niiler, and H. Valdimarsson, 2003: North Atlantic Ocean surface currents. *J. Geophys. Res.*, **108**, 3002, doi:10.1029/2001JC001020.
- Rudels, B., P. Eriksson, H. Gronvall, R. Hietala, and J. Launiainen, 1999: Hydrographic observations in Denmark Strait in fall 1997, and their implications for the entrainment into the overflow plume. *Geophys. Res. Lett.*, **26**, 1325–1328.
- , E. Fahrbach, J. Meincke, G. Budeus, and P. Eriksson, 2002: The East Greenland Current and its contribution to the Denmark Strait overflow. *ICES J. Mar. Sci.*, **59**, 1133–1154.
- Schmitz, W. J., and M. S. McCartney, 1993: On the North Atlantic circulation. *Rev. Geophys.*, **31**, 29–49.
- Steffansson, U., 1962: North Icelandic waters. *Rit. Fiskideild.*, **3**, 1–269.
- Straneo, F., M. Kawase, and R. S. Pickart, 2001: Effect of wind on convection in strongly and weakly baroclinic flows with application to the Labrador Sea. *J. Phys. Oceanogr.*, **32**, 2603–2618.
- Talley, L. D., and M. S. McCartney, 1982: Distribution and circulation of Labrador Sea Water. *J. Phys. Oceanogr.*, **12**, 1189–1205.
- Thomas, L., and C. M. Lee, 2005: Intensification of ocean fronts by down-front winds. *J. Phys. Oceanogr.*, **35**, 1086–1102.
- Torres, D. J., and C. Mauritzen, 2002: Using a global tidal model for removing tides from direct velocity measurements in the Faroe Bank Channel. *Amer. Geophys. Union*, **82**, OS32F-197.
- Worthington, L. V., 1970: The Norwegian Sea as a Mediterranean basin. *Deep-Sea Res.*, **17**, 77–84.